Journal of Inorganic and Organometallic Polymers and Materials
https://doi.org/10.1007/s10904-024-03104-5

RESEARCH

Nano-Spheroidal MnOx/C Nanomaterial with Battery-Like and Capacitive Charge Storage for Lithium-Ion Capacitors

Cuimei Zhao[1] · Siyu Jiang[1] · Songlin Tian[1] · Xiangxin Xue[1] · Ping Nie[1] · Limin Chang[1]

Received: 27 November 2023 / Accepted: 13 April 2024

Abstract
Lithium-ion capacitors (LICs) possess the potential to satisfy the demands of both high power and energy density for energy storage devices. In this report, a novel LIC has been designed featuring with the MnOx/C batterytype anode and activated carbon (AC) capacitortype cathode. The Nano-spheroidal MnOx/C is synthesized using facile one-step combustion method. Benefiting from the uniform distribution of the MnOx/C nano-spheroidal particle, a fast kinetics for both charge-transfer and ion-diffusion process is realized, promoting battery-like and capacitive energy storage. As anticipated, the MnOx/C composite material exhibits an exceptional capacity of 1167.2 and 828.5 mAh g^{-1} from the first and the 100th cycle at 0.1 A g^{-1}, high rate capability of 171.1 mAh g^{-1} even at a high rate of 2 A g^{-1}, much higher than pure MnOx. The MnOx/C//AC LIC displays an excellent electrochemical performance with excellent energy density of 66.9 Wh kg^{-1} (250 W kg^{-1}) and remarkable power density of 2500 W kg^{-1} (11.7 Wh kg^{-1}). These encouraging results make the electrode material and electrode system promising for nextgeneration highperformance energy storage devices.

Keywords Lithium-ion capacitors · Energy storage · Energy density · Power density

1 Introduction

Energy crisis and environmental pollution have become the serious problems around the world [1–3]. There is an urgent need to develop advanced energy storage/conversion devices with both high energy and power density. Among the various devices, batteries and supercapacitors are two prominent electrochemical energy storage/conversion technologies. Unfortunately, current energy storage devices have certain limitations, such as low power density for batteries and low energy density for supercapacitors [4, 5]. As a hybrid energy storage/conversion device, lithium-ion capacitor (LIC) has emerged as a promising hybrid system, that combine high energy density of battery-type anodes (lithium ion insertion/extraction reactions) and the high power density of capacitor-type cathodes (rapid ion adsorption/desorption) [6–11].

Actually, the drawbacks of slow kinetics and low specific surface area for the anode materials lead to the LICs remaining lower energy and power density. It remains a significant challenge to develop a high-performance anode material with fast kinetics and high activity for both charge-transfer and ion-diffusion. Therefore, considerable attention has been devoted to developing suitable Li-insertion anode materials that satisfy requirements for both charge-transfer and ion-diffusion. As expected, Lithium-based inorganic or organic compounds have achieved relatively high energy storage properties, such as $LiMn_2O_4$, Li_3VO_4, Li_5FeO_4, Li_6CoO_4, $Li_{0.65}Ni_{1.35}O_2$ and so on [10–17]. However, all the above lithium-based compounds display several shortcomings, including low specific capacity, high prelithiation potential, poor rate capacitance and low security. For example, $LiMn_2O_4$ nano-cubes material was synthesized by a template-engaged reaction method, which displayed discharge specific capacity of 95.39 mAh g^{-1} with a capacity retention of 90.91% after 500 cycles at 100 mAg^{-1} [14]. The

✉ Cuimei Zhao
xiaocuier1112@126.com

✉ Ping Nie
pingnie@jlnu.edu.cn

✉ Limin Chang
changlimin2139@163.com

[1] Key Laboratory of Preparation and Applications of Environmental Friendly Materials, Ministry of Education, College of Chemistry, Jilin Normal University, Changchun 130103, PR China

Published online: 09 May 2024

relative low capacity and complex preparation method limit its wide application. Fortunately, transition metal oxides [18–20] and dichalcogenides [21–27] possess high theoretical capacity (450–1500 $mAhg^{-1}$) and excellent safety, such as Nb_2O_5, TiO_2, WS_2 and so on. However, most battery electrode materials, especially metal oxides, undergo significant volume changes during Li-ion insertion/extraction processes which result in poor cyclic stability and low rate capacitance [28, 29]. The ideal LICs electrode materials should have high conductivity, short charge transfer path, and minimal volume expansion. Among the various battery materials, MnOx materials such as Mn_3O_4, MnO_2 and MnO, have become a reserch hotspot of LIC electrode material due to its advantage of non-toxic, low-cost and abundant in nature. However, the defects of poor conductivity and volume expansion associated with metal oxide electrodes also impede their widespread application. In order to improve the conductivity and activity, Mn_3O_4/graphene anode nanocomposites were prepared by two-step hydrothermal process. Mn_3O_4-graphene composite electrode exhibited a reversible specific capacity of 474 mAh g^{-1} at 100 mA g^{-1} upon 200 cycles [30].

In order to further improve the energy storage properties, we combined MnOx with carbon using a facile one-step combustion synthesis. The highly conductive carbon material can provide fast electron transport and the highly active MnOx material can provide efficient charge exchange and storage. Benefiting from battery-like and capacitive charge storage, the MnOx/C composite material exhibits high capacity, rate capability and cycling stability. Additionally, a new lithiumion capacitor has been designed with the MnOx/C batterytype cathode and activated carbon (AC) capacitortype anode, showing an excellent electrochemical performance with high energy and power density. This work will provide new insight into the design and application of high-performance energy storage material and device.

2 Experimental

2.1 Preparation of MnOx/C Electrode

For anode preparation, the MnOx/C composite material was synthesized by one-step combustion method. In the synthesis, manganese acetate ($C_4H_6MnO_4$•$4H_2O$) was dispersed in anhydrous ethanol (C_2H_5OH) by evenly stirring (the weight ratio of $C_4H_6MnO_4$•$4H_2O$/C_2H_5OH was 1:30, 1:40, 1:50). Then, the obtained transparent solution was ignited until the manganese acetate converted into MnOx and the carbon material embedded into MnOx by the incomplete combustion. The obtained material were named as MnOx/C-30, MnOx/C-40 and MnOx/C-50, respectively. For comparison, MnOx was synthesized using the calcination of $C_4H_6MnO_4$•$4H_2O$ at 350 ℃ for 3 h.

The MnOx/C or MnOx power (85 wt%) was mixed with conductive black (10 wt%) and polyvinylidene fluoride binder (5 wt%), in N-methyl pyrrolidone solutions then coated on a Cu foil, and fnally dried at 70℃ in vacuum to obtain the MnOx/C or MnOx electrode.

2.2 Preparation of AC Electrode

To prepare cathode, the AC electrode was prepared by a simple slurry coating technique. AC (85 wt%), acetylene black (10 wt%), and polyvinylidene fluoride binder (5 wt%), thoroughly mixed in N-methyl pyrrolidinone solution (NMP) to form a black slurry. It was then evenly pasted on the Al foil. After drying in vacuum, an AC electrode was obtained.

2.3 Fabrication of Lithium-Ion Capacitors

The Lithium-Ion Capacitors half-cell or full-cell was fabricated using polypropylene film as the separator in 2025 coin-type cells. The employed electrolyte was 1 M $LiPF_6$ in ethylene carbonate, ethyl methyl carbonate and dimethyl carbonate (EC/EMC/DMC, v/v/v = 1:1:1) solution. For the half-cell test, MnOx/C electrode or AC electrode assembled with Li foil as both counter and reference electrodes has been conducted. LIC full-cell was assembled with the MnOx/C electrode and AC electrode serving as the anode and cathode. The mass loading of MnOx/C and AC was 1 mg cm^{-2} and 2 mg cm^{-2}, respectively .

2.4 Characterization

The surface morphology was examined using scanning electron microscopy (SEM, JEOL 6700 F), the surface areas was tested by Brunauer-Emmett-Teller (BET, Autosorb-iQ), the chemical composition was determined through X-ray diffraction (XRD, RIGAKU D/MAX2500PC), and elemental bonding was observed via X-ray photoelectron spectroscopy (XPS, ESCALAB-250Xi). Furthermore, the electrochemical performance was analyzed using a computer-controlled electrochemical working station (CHI660E or Land CT-2001 A).

3 Results and Discussion

The XRD patterns of MnOx and MnOx/C nanomaterials are illustrated in Fig. 1(a). As observed from the figure, the patterns for MnOx/C and MnOx exhibit some similarities. The prominent peaks locating at 18.0°, 28.9°, 32.3°, 36.1°, 44.4°, 50.8°and 59.9° can be attributed to (101), (112), (103), (211),

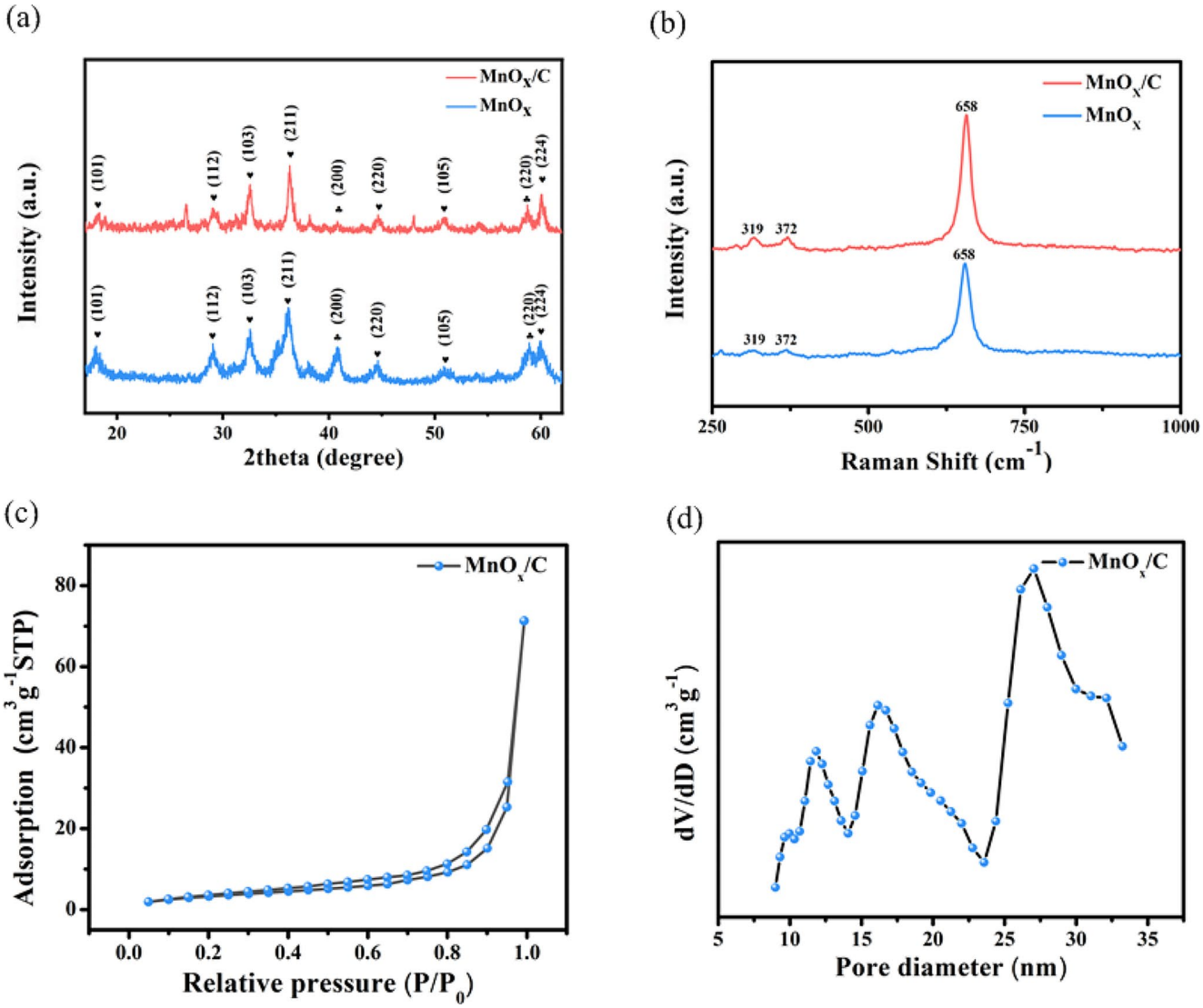

Fig. 1 (**a**) X-ray diffraction patterns and (**b**) Raman spectrum of MnOx/C and MnOx; (**c**) N_2 adsorption-desorption isotherm plot and (**d**) pore size distribution of MnOx/C

(220), (105), and (224) planes of rhodochrome-type Mn_3O_4 (JCPDS card no. 24–0734) [31, 32]. Additionally, weak peaks at 40.9° and 59.0° correspond to the (200) and (220) facets of MnO (JCPDS No. 07-0230) [33, 34]. However, for MnOx/C composites, there are additional weak peaks at 26.3°, which can be indexed to hexagonal carbon materials (JCPDS card No. 41-1487). The absence of obvious diffraction peak for both MnO and carbon in the XRD patterns of MnOx/C composites may be due to their small amount present in the sample. Notably, the broadening of these peaks suggests an amorphous structure in the MnOx or MnOx/C material, which could be beneficial to an enhanced electrochemical activity. Raman spectrum for MnOx and MnOx/C are shown in Fig. 1(b). A sharp peak observed at 658 cm^{-1} and two small peaks at 319 and 372 cm^{-1} are characteristic of Mn_3O_4, further confirmed the existence of the spinel structure of Mn_3O_4 [35, 36]. The N_2 adsorption-desorption isotherm plots of MnOx/C are presented in Fig. 1(c) and (d). The sample displays type-IV isotherm according to the IUPAC classification, characteristic of a mesoporous material with BET surface areas of 12.216 m^2g^{-1} (Fig. 1(c)). The MnOx/C material possesses plentiful mesopores with pore sizes in the ranges of 10–20 and 25–35 nm (Fig. 1(d)). The porous structure is conducive to the transport and storage of electrolyte ions, which can improve the pseudocapacitance performance of the composite electrode.

The TEM images of MnOx and MnOx/C presented in Fig. 2(a) and (b) demonstrate that while both samples possess spherical structures, MnOx/C nanoparticles have a smaller average diameter around 20 nm compared to pure MnOx. Moreover, MnOx/C nanoparticles display better homogeneity with less agglomeration than pure MnOx.

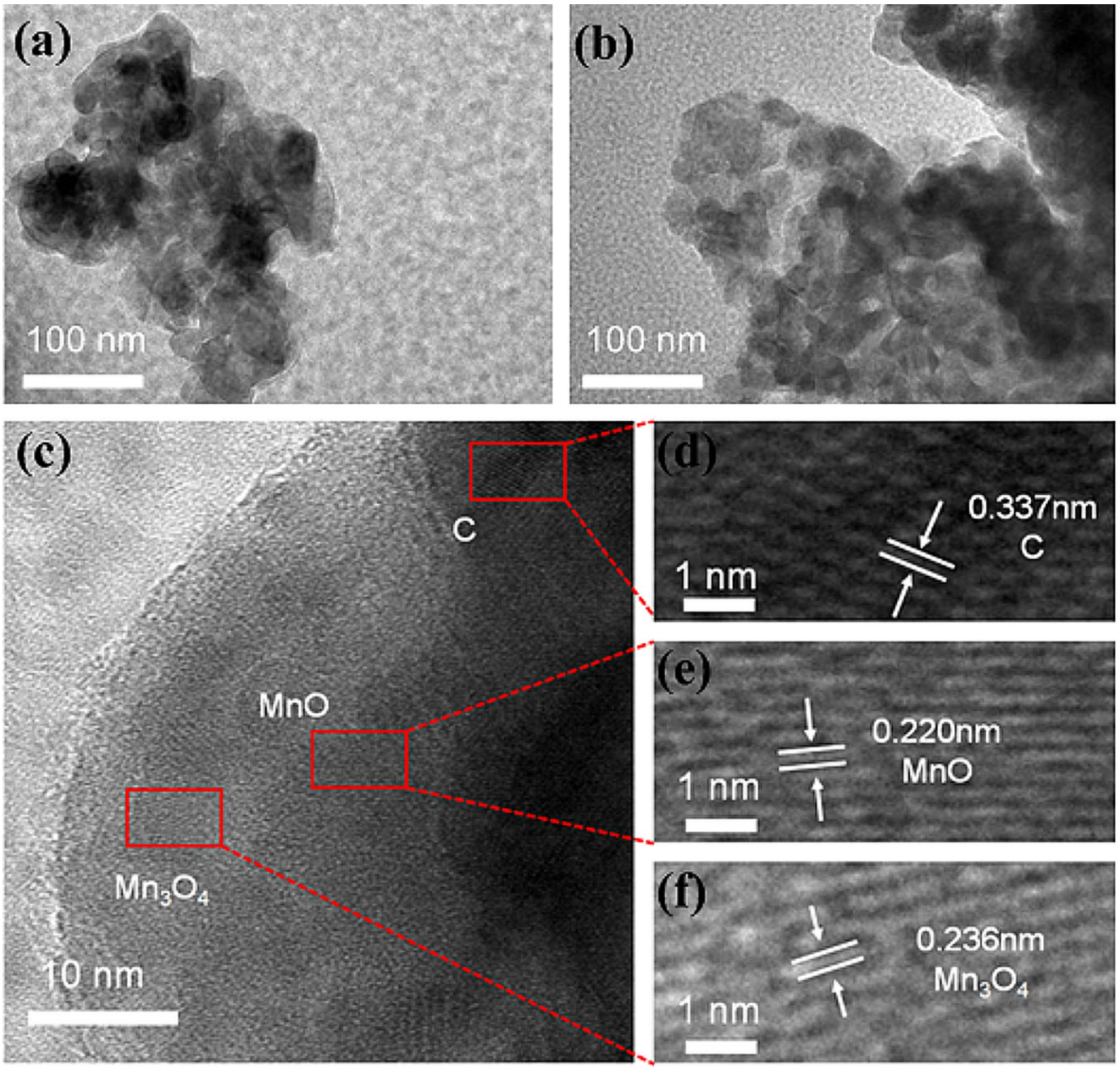

Fig. 2 TEM image of (**a**) MnOx and (**b**) MnOx/C; (**c**) HR-TEM images of MnOx/C; (**d**) HR-TEM images of C, (**e**) MnO and (**f**) Mn_3O_4 in MnOx/C composite

Therefore, MnOx/C nanomaterials could provide more efficient active storage sites along with shorter ion transmission paths. The high-magnified TEM images for MnOx/C shown in Fig. 2(c)-(f) further reveal the d-spacing values of 0.337 nm, 0.220 nm and 0.236 nm, which correspond respectively to (002) plane of C, (200) plane of MnO, and (004) plane of Mn_3O_4, indicating the synthesis of C, MnO and Mn_3O_4 in MnOx/C nanoparticles. The results obtained from HR-TEM analysis are consistent with the XRD patterns.

Figure 3(a) and (b) shows the SEM image of MnOx/C nanomaterials, consisting of a number of uniformly distributed spherical particles, which are interconnected and tightly gathered together to form a nest-like porous structure. This surface morphology not only can increase the specific surface area of the whole material, but also enhance the transport and conduction of Li^+, which would be favorable to the fabrication of high capacity electrode materials toward practical applications in LICs. The X-ray spectroscopy EDS analysis in Fig. 3(c) reveals that the MnOx/C nanomaterials consist of Mn, O and C elements. Moreover, the EDS

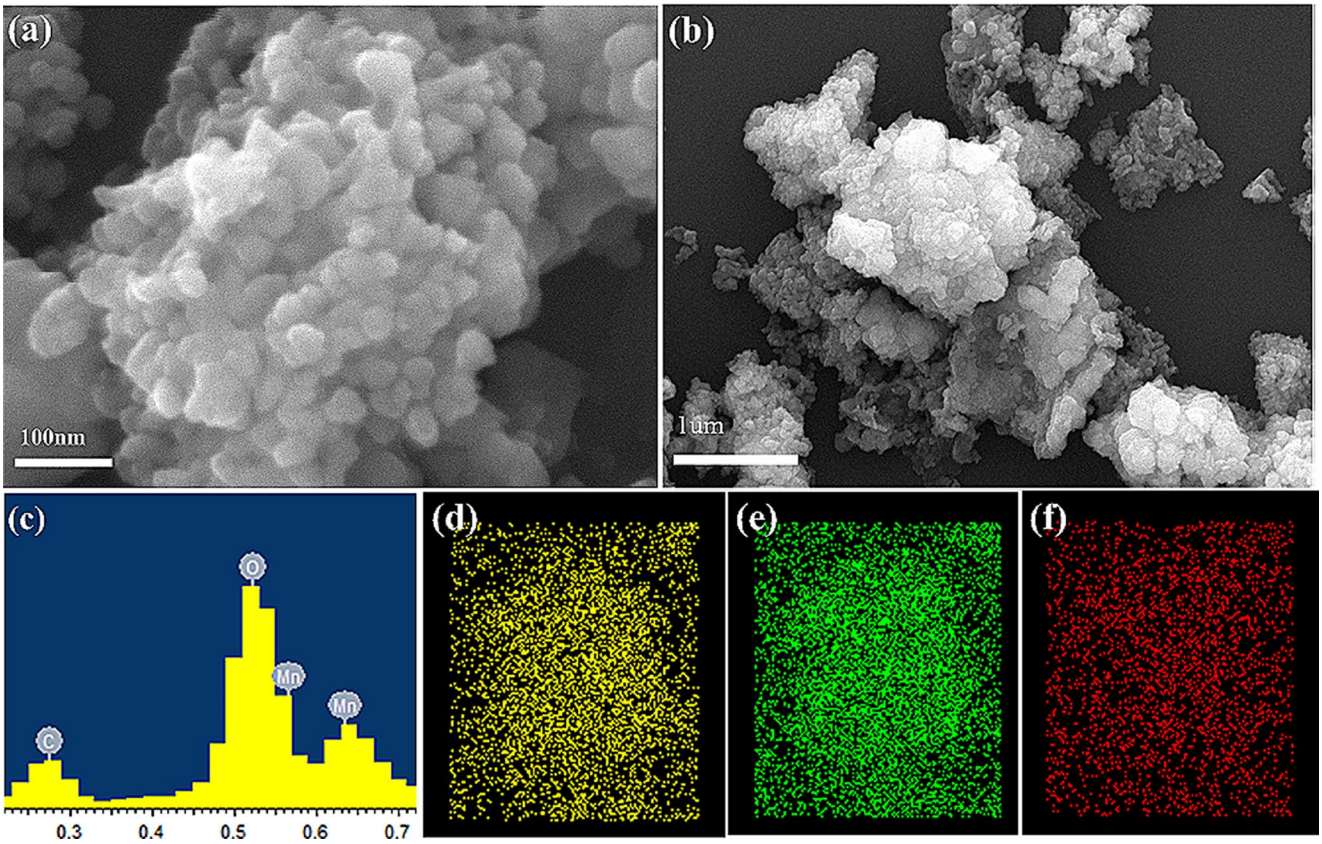

Fig. 3 (**a**, **b**) SEM (top view) images of MnOx/C, (**c**) EDS image of MnOx/C and (**d**, **e**, **f**) Elemental mapping results of MnOx/C

elemental mapping images in Fig. 1(d)-(f) also demonstrate a uniform distribution of Mn (yellow), O (green) and C (red) in MnOx/C composites.

The full XPS spectrum of MnOx/C is presented in Fig. 4(a), revealing the presence of Mn, O, and C elements in the MnOx/C composite. The spectrum of O 1s in Fig. 4(b) exhibits two peaks at 530.0, and 531.3 eV, corresponding to the Mn-O-Mn bond and the Mn-O-H bond [37, 38]. The characteristic double peaks observed in Fig. 4(c) at approximately 642 eV (Mn 2p 3/2) and 654 eV (Mn 2p 1/2), are consistent with previously reported results for MnOx based on differences in binding energies [39]. Additionally, Fig. 4(d) displays C1s peaks at 284.6, 285.4, and 288.8 eV, representing sp2-hybridized carbon, sp3-hybridized carbon, and O = C-O, respectively [37]. Thus, these test results corroborate the findings from the XRD, EDS and HR-TEM analysis and confirm the existence of both MnOx and carbon within the MnOx/C composite material.

The electrochemical performance of samples was evaluated through cyclic voltammetry (CV), galvanostatic charge-discharge (GCD) and electrochemical impedance spectrometry (EIS) measurements. To coordinate the MnOx/C anode, we prepared AC cathode and investigated its electrochemical performance in a Li-half cell system operating between 2 and 4.3 V vs. Li/Li^+. Figure 5(a) illustrates the CV curves of the AC cathode at different scanning rates ranging from 2 to 50 mVs^{-1}. These curves exhibit rectangular shapes indicative typical double-layer capacitance behavior. Figure 5(b) presents GCD measurements of the AC cathode conducted at various current densities from 0.1 to 2 Ag^{-1}, in which all profiles demonstrate linearity and symmetry, further confirming the excellent EDLC behavior provided by rapid ion adsorption/desorption. From Fig. 5(c) at a current density of 0.1 Ag^{-1}, initial discharge capacity is measured as 55 $mAhg^{-1}$ corresponding with charge capacity of 62 $mAhg^{-1}$, exhibiting an initial coulombic efficiency value of approximately 88.7%. With increasing current densities to the values of 0.2, 0.5, 1 and 2Ag^{-1}, the discharge capacities for the AC cathode remain at 48.4, 42.4, 37.7 and 33.4 $mAhg^{-1}$, respectively, demonstrating an excellent rate capacity of the AC cathode. Figure 5(d) illustrates cycling life and coulombic efficiency of the AC cathode at 1 Ag^{-1}. Even after undergoing 2000 cycles, it can still exhibits an impressive discharge capacity of 37.1 $mAhg^{-1}$, with a capacitance retention of 94.9% and a coulombic efficiency of 98.9%, thereby demonstrating its exceptional stability and reversibility. Based on these findings, it can be inferred that the AC could be a promising cathode material for LICs,

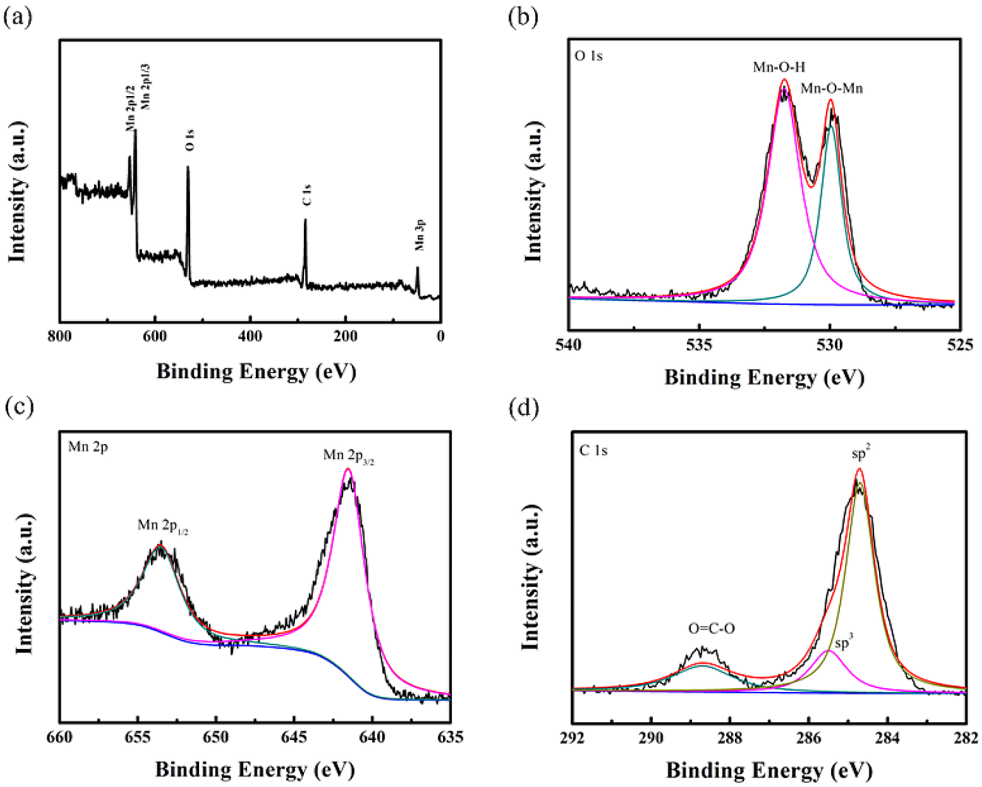

Fig. 4 (**a**) XPS wide survey spectrum and (**b**) O 2p, (**c**) Mn 2p, and (**d**) C 1 s spectra of MnOx/C

which could provide high power density and stable cycling performance through efficient adsorption/desorption of anions [40, 41].

To evaluate the lithium storage performance of MnOx/C materials, a half-cell was assembled with a lithium sheet anode and a MnOx/C or MnOx cathode. The electrochemical property of MnOx/C (including MnOx/C-30, MnOx/C-40 and MnOx/C-50) or MnOx tested at different current densities of 0.1、0.2、0.5、1、2 and 0.1 A g^{-1} are shown in Fig. 6(a). The capacity of the MnOx/C-40 shows a high energy storage property, with a capacity of 621.8、487.4、372.8、288.6、171.1 and 622.5 mAh g^{-1}, respectively, more outstanding than that for pure MnOx of 477.2、324.1、226.5、160.8、102.6 and 419.1 mAh g^{-1}, respectively. Therefore, we selected MnOx/C-40 (marked as MnOx/C) to explore the electrochemical performance. The high rate capacitance for MnOx/C can be attributed to the improvement of lithium ion diffusion ability to improve the reversibility of energy storage.

The comparison of cycling stability for MnOx/C and MnOx during charge/discharge processes at 0.1 A g^{-1} is illustrated in Fig. 6(b). After completing 100 cycles, the MnOx/C material still demonstrates a high specific capacity of 828.5 mAh g^{-1}, corresponding to 71.0% capacity retention, which is apparently higher than the pure MnOx (267.3 mAh g^{-1}, 24.3%). Furthermore, the coulombic efficiency for MnOx/C can keep 100%, displaying an outstanding energy storage properties. The observed cyclic behavior reveals an initial decrease followed by subsequent increase in capacity during each cycle. This trend can be attributed to the formation and rupture process of the solid electrolyte interface (SEI) film upon initial charge/discharge cycle [42, 43]. The high cyclic stability of MnOx/C can be attributed to both the high activity of MnOx and the excellent electron conductivity of the carbon material, which synergistically enable efficient lithium ion insertion and ejection.

The Fig. 7(a) shows the 1st, 2nd, 3rd, 5th and 10th GCD curves of MnOx/C electrode at 0.1 A g^{-1} within a voltage range from between 0 and 3.0 V to systematically evaluate charging/discharging behavior of MnOx/C. The first cycle delivers a discharge capacity of 708.5 mAh g^{-1} along with a charge capacity of 1167.2 mAh g^{-1}, concomitant with an initial coulomb efficiency of 60.7%. The irreversible capacity observed in the first cycle is primarily caused by the formation of SEI film in the battery. Subsequently, the MnOx/C material displays a high invertible discharge capacity of 697.0 mAh g^{-1} from the second cycle onwards, accompanied by a rapid increase in coulombic efficiencies up to 94.4%, suggesting an efficient Li^+ insertion/extraction behavior. Furthermore, the discharge-charge curves exhibit little change from the third to tenth cycle, confirming the good cycling stability for the MnOx/C materials, which could be partly attributed to an activation process.

The CV curves of MnOx/C at various sweep rates ranging from 0.1 to 2.0 mV s^{-1} are depicted in Fig. 7(b). From the CV curve at 1.0 mVs^{-1}, the voltage peak observed at

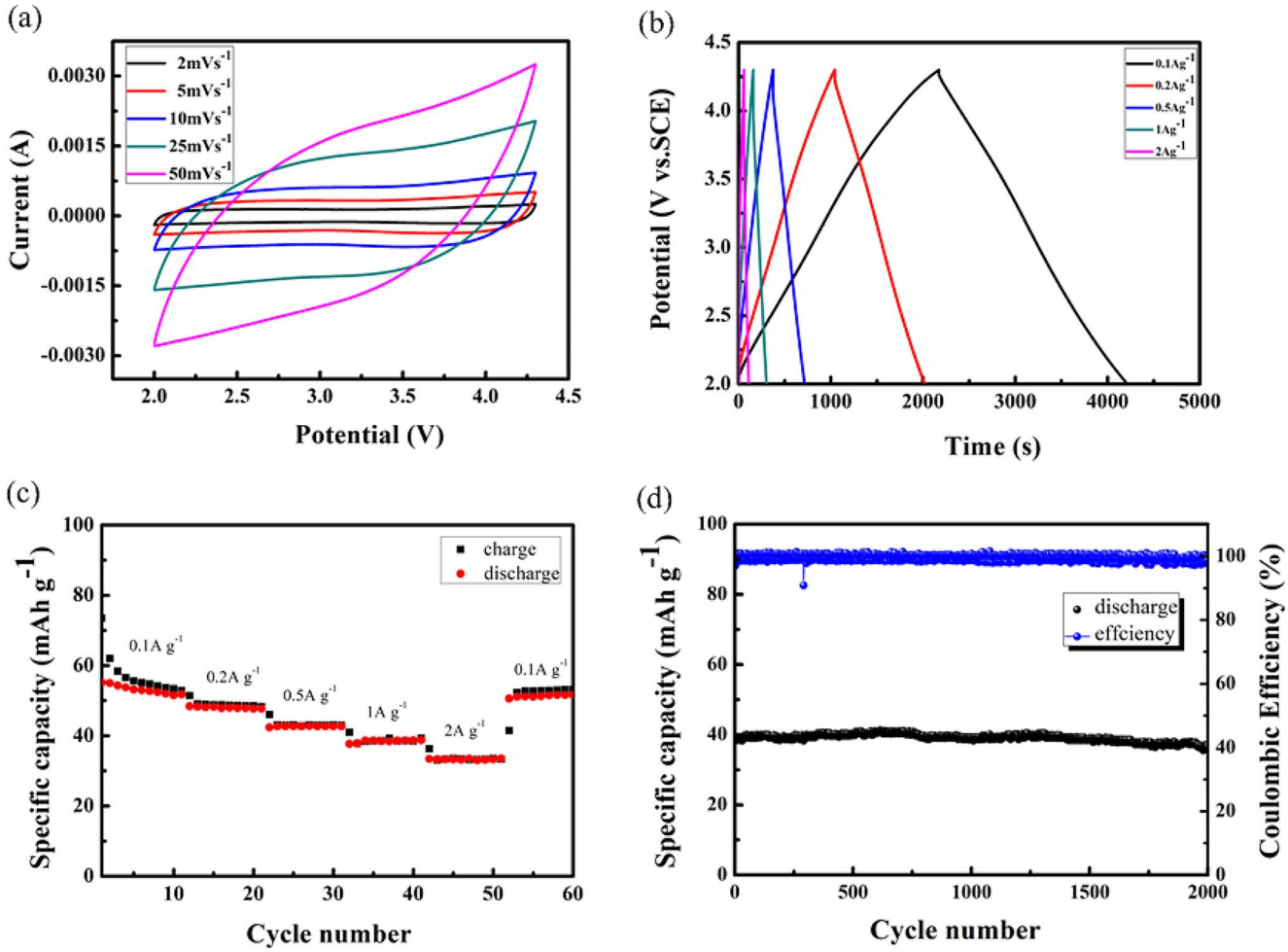

Fig. 5 Electrochemical properties of AC cathode: (**a**) CV curves at different scan rates, (**b**) GCD curves at different current densities, (**c**) Rate performance at different current density, (**d**) Cycling performances at current 1 A g^{-1}

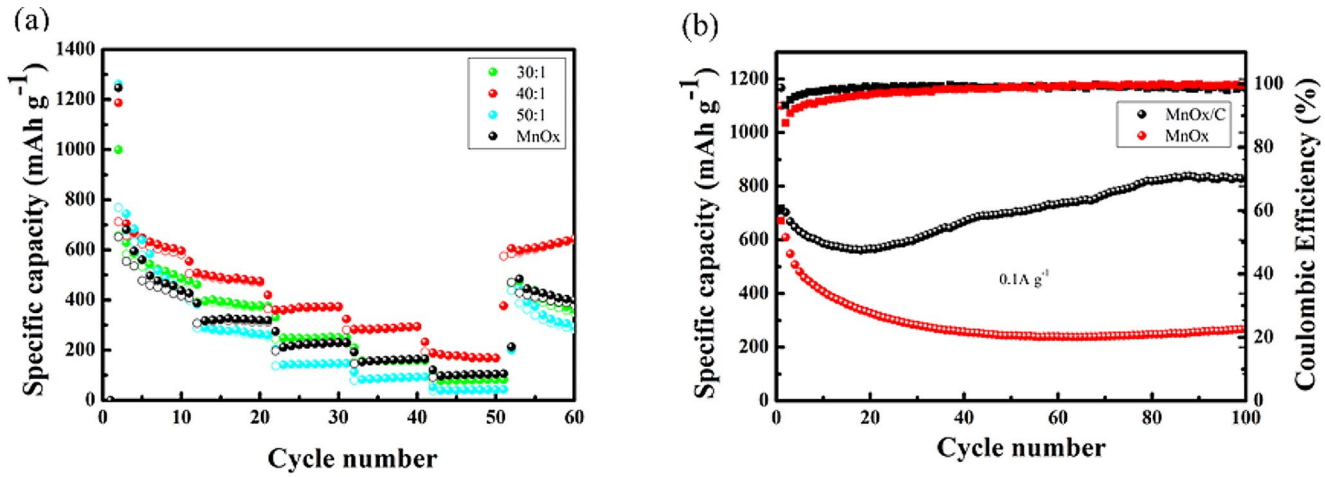

Fig. 6 (**a**) Rate performance at different current densities and (**b**) Cycling performances at 0.1 A g^{-1} of MnOx/C and MnOx

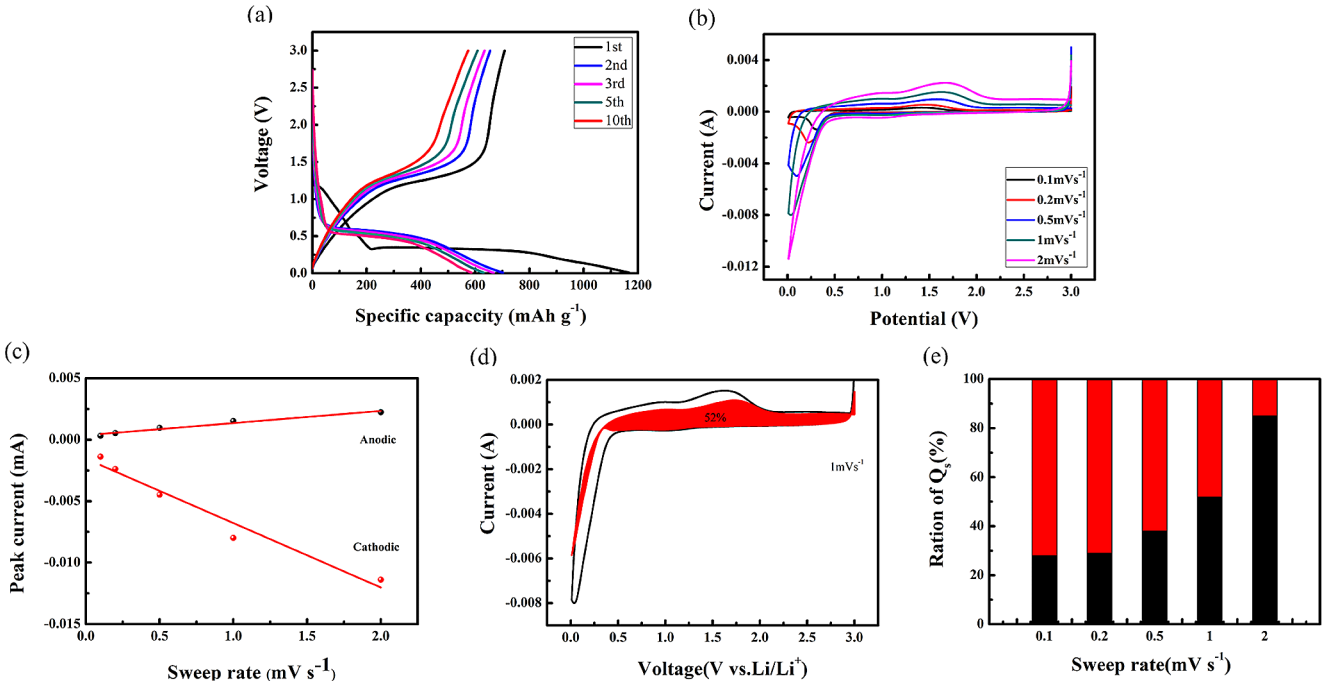

Fig. 7 (**a**) GCD curves at 0.1 A g^{-1} and (**b**) CV curves at different scan rates of MnOx/C; (**c**) Relationship between the peak currents and potential sweep rates, (**d**) CV curve with sweep speed of 1 mV s^{-1} (the shaded area corresponds to the estimated pseudocapacitance contribution) and (**e**) the contribution ratio of capacitive and diffusion-controlled behaviors versus scan rate of MnOx/C

0.03 V can be attributed to the electrochemical reaction involving the formation of Mn and Li_2O, corresponding to the battery-like reaction of MnO_x + 2x Li++2x e-→Mn (0)+x Li_2O [44]. Additionally, the anodic peak observed at 1.6 V corresponds to the conversion reaction.

$$i = a * v^b \tag{1}$$

$$Log\,(i) = b * Log\,(v) + Log\,(a) \tag{2}$$

$$i\,(V) = k_1 * v + k_2 * v^{\frac{1}{2}} \tag{3}$$

Notably, as the sweep rate increases, both anodic and cathodic processes exhibit a linear relationship between peak current and sweep rate, indicating a high energy storage property (Fig. 7(c)). According to Eqs. 1–3, the specific contributions of the capacitive behavior (k_1v) and the diffusion-controlled behavior ($k_2v^{1/2}$) at different scan rates have been calculated. As shown in Fig. 7(d), the capacitance contribution ratio at the scanning rate of 1.0 mV s^{-1} is 52% obtained by CV curve. And with the increasing of scan rate from 0.1 to 2.0 mV s^{-1}, the contribution ratios of capacitance increase from 28 to 85% (Fig. 7(e)). The capacitive characteristics enable fast charging and discharging rates, demonstrating high power characteristic of the MnOx/C composite.

In summary, the high energy storage property for MnOx/C composite can be collectively attributed to the following factors: the highly conductive carbon material provides rapid and effective electron transport, therefore high electrochemical stability and rate capacitance can be expect; The uniform distribution of spherical particles promote the deep ions diffusion and high utilization of active electrode material, consequently high capacity performance can be achieved.

To further assess the feasibility of the MnOx/C composite for the energy conversion/storage application, we fabricated MnOx/C//AC LIC with the MnOx/C anode and the AC cathode. The electrochemical reaction mechanism of MnOx/C//AC LIC is illustrated in Fig. 8(a). According to the principle of charge balance [45, 46], the mass ratio between the cathode and the anode is maintained at 2:1. Under these conditions, their CV curves of the LIC in Fig. 8(b) are retained a similar shape as the scan rate increased from 2 to 50 mV s^{-1}, indicating an excellent energy-storage behavior. By employing this design, the working voltage of the assembled LIC device can reach up to 3.0 V. Additionally, slight deviations from rectangular shape were observed in the CV curves due to coupling effects arising from different energy storage mechanisms between capacitor-type cathode and battery-type anode.

The GCD curves in Fig. 8(c) displays excellent linear and symmetric feature, further confirming ideal electrochemical reversibility and low equivalent series resistance of the MnOx/C//AC LIC. Based on the GCD curves, the specific capacitance values are 32.1, 22.9, 11.9 and 5.6 Fg^{-1}

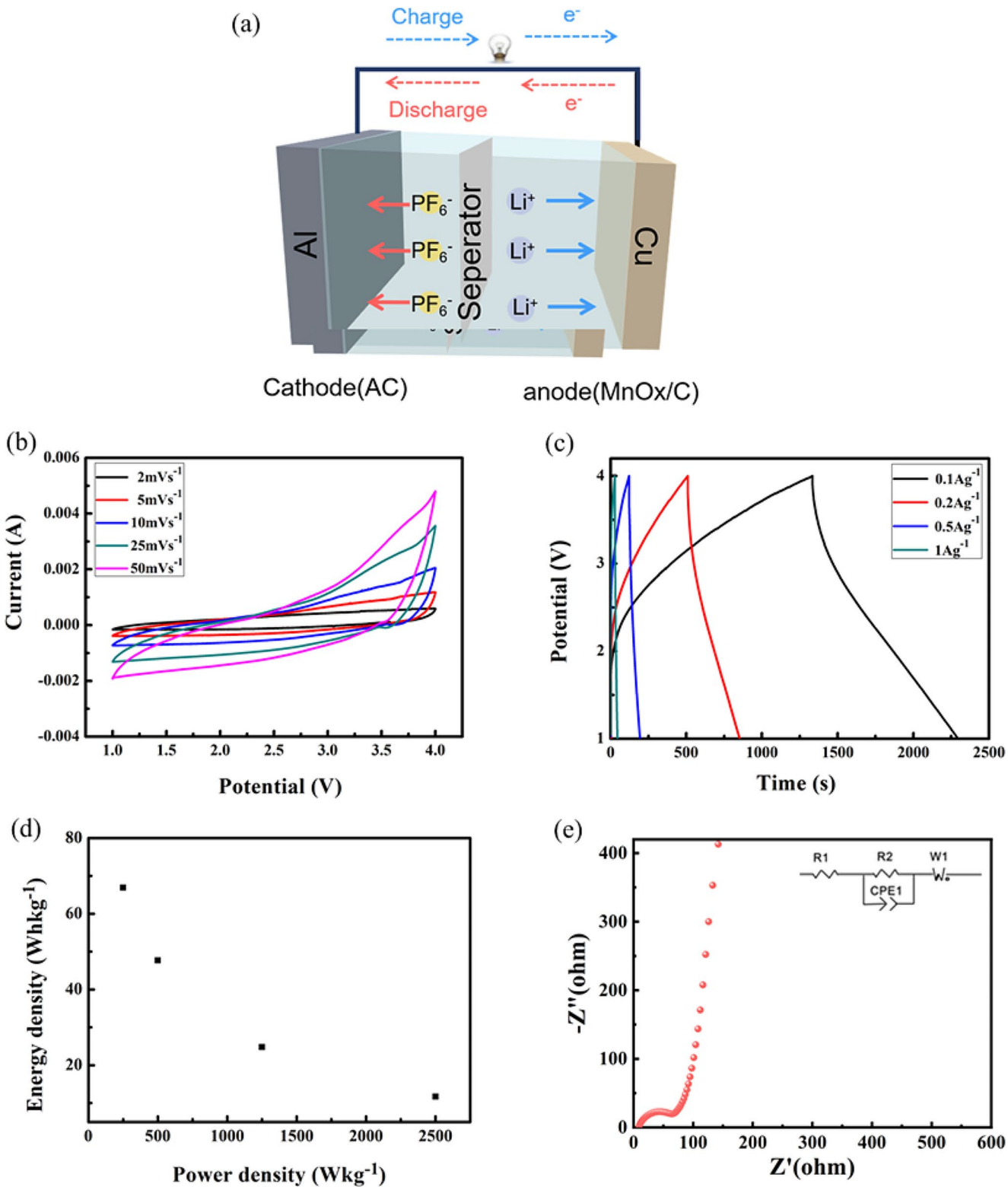

Fig. 8 (**a**) Schematic illustration for charge storage, (**b**) CV curves of the LIC at different scan rates, (**c**) GCD curves at different current densities, (**d**) Ragone plot and (**e**) Electrochemical impedance spectra for the MnOx-C//AC LIC

at 0.1, 0.2, 0.5 and 1 Ag^{-1}, respectively. The energy density and power density of the LIC device were also measured. The results of Ragone plot are illustrated in Fig. 8(d). It is noteworthy that the LIC device demonstrates a high energy density of 66.9 Wkg^{-1} at a power density of 250 Wkg^{-1}, while still maintaining an energy density of 11.7 $Whkg^{-1}$ even at a high power density of 2500 Wkg^{-1}.The obtained specific energy and power values are better than those of the reported earlier LICs, including Cu-HCF//GC (42.78$Whkg^{-1}$ at 523.89 Wkg^{-1}) [5], CNT/V_2O_5//AC (40 $Whkg^{-1}$ at 210 Wkg^{-1}) [47], $LiCO_2$//AC (25 $Whkg^{-1}$ at 74 Wkg^{-1} [48], soft carbon//AC/Li_3N (74.7 $Whkg^{-1}$ at 75.1 Wkg^{-1} [49], and MoS_2/NiS//AC (31 $Whkg^{-1}$ at 155.7 Wkg^{-1}) [50]. Furthermore, the EIS result for the LIC device is showed in Fig. 8(e). The charge transfer resistance of the LIC device is small, suggesting a fast transport of electron; The straight line in the low-frequency region shows a larger slope, indicating an excellent diffusion of ions. The excellent energy storage performance is attributed the efficient charge storage mechanism from batterytype anode and capacitortype cathode, and the synergistic effect between the two electrodes.

4 Conclusions

The MnOx/C electrodes have been prepared via a facile and cost-effective one-step combustion synthesis method. Benefiting from the electrochemical activity, and electrical conductivity of the MnOx/C composite, the MnOx/C electrode exhibits a maximum capacity of 1167.2 mAh g^{-1} at 0.1 A g^{-1} with excellent rate capability and cycling stability. The high capacity of the MnOx/C nanomaterial arises from the battery-type energy storage mechanism involving lithium ion insertion/extraction reactions, while its exceptional cyclic stability and rate capability stem from capacitive charge storage mechanism through rapid ion adsorption/desorption. Furthermore, the assembled MnOx/C//AC LIC exhibits a remarkable energy density of 66.9 Wkg^{-1} at a power density of 250 Wkg^{-1}, and it even maintains an impressive energy density of 11.7 $Whkg^{-1}$ at a high power density of 2500 Wkg^{-1}. The energy storage material and device demonstrate great potential for practical applications.

Acknowledgements Science and Technology Development Plan Project of Jilin Province (No. YDZJ202101ZYTS187, YDZJ202201ZYTS615), the Projects of Jilin Province Department of Education (No. JJKH20220443KJ, JJKH20230499KJ), and the National Natural Science Foundation of China (No.52072145) are highly appreciated.

Author Contributions Conceptualization, C.Z.; Funding acquisition, C.Z.and L.C; Investigation, S.J. and S.T.; Supervision, P.N.; Validation, P.N.; Visualization, S.T.; Writing-original draft, C.Z. and S.J.; Writing-review and editing, S.T. and X.X. All authors have read and agreed to the published version of the manuscript.

Data Availability No datasets were generated or analysed during the current study.

Declarations

Competing Interests The authors declare no competing interests.

References

1. S. Yuan, Q. Lai, X. Duan, Q. Wang, Carbon-based materials as anode materials for lithium-ion batteries and lithium-ion capacitors: a review. J. Energy Storage. **61**, 106716 (2023)
2. Y. Chen, Y. Kang, Y. Zhao, L. Wang, J. Liu, Y. Li, Z. Liang, X. He, X. Li, N. Tavajohi, A review of lithium-ion battery safety concerns: the issues, strategies, and testing standards. J. Energy Chem. **59**, 83–99 (2021)
3. G. Xu, G.Y. Wang, X.F. Zhang, Z.P. Deng, L.H. Huo, S. Gao, Biotemplate synthesis of mesoporous α-Fe_2O_3 hierarchical structure with assisted pseudocapacitive as an anode for long-life lithium ion batteries. Ceram. Int. **47**, 3772–3779 (2021)
4. K.M.A. Raihan, S. Sahoo, T. Nagaraia, S. Sigder, B. LaCroix, C.M. Sorensen, S.R. Das, Transforming scalable synthesis of graphene aerosol gel material toward highly flexible and wide-temperature tolerant printed micro-supercapacitors. APL Energy. **2**, 016104 (2024)
5. P. Pazhamalai, K. Krishnamoorthy, S. Sahoo, S.J. Kim, High-energy aqueous Li-ion hybrid capacitor based on metal-organicframework-mimicking insertion-type copper hexacyanoferrate and capacitive-type graphitic carbon electrodes. J. Alloy Compound. **765**, 1041–1048 (2018)
6. T. Li, G. Yu, M. Song, Q. Zhang, Y. Li, X. Bai, Facile synthesis of Nb-Doped $CoTiO_3$ hexagonal microprisms as Promising Anode materials for Lithium-ion batteries. Inorganics. **11**, 10 (2023)
7. F. Bonaccorso, L. Colombo, G. Yu, M. Stoller, V. Tozzini, A.C. Ferrari, R.S. Ruoff, V. Pellegrini, Graphene, related two-dimensional crystals, and hybrid systems for energy conversion and storage. Science. **347**, 1246501 (2015)
8. M.S. Dresselhaus, I.L. Thomas, Alternative energy technologies. Nature. **414**, 332–337 (2001)
9. J. Ding, W. Hu, E. Paek, D. Mitlin, Review of hybrid ion capacitors: from aqueous to lithium to sodium. Chem. Rev. **118**(14), 6457–6498 (2018)
10. L. Wang, X. Zhang, C. Li, X.Z. Sun, K. Wang, F.Y. Su, F.Y. Liu, Y.W. Ma, Recent advances in transition metal chalcogenides for lithium-ion capacitors. Rare Met. **41**, 2971–2984 (2022)
11. S. Yuan, X. Duan, J. Liu, Y. Ye, F. Lv, T. Liu, Q. Wang, X. Zhang, Recent progress on transition metal oxides as advanced materials for energy conversion and storage. Energy Storage Mater. **42**, 317–369 (2021)
12. C. Sun, X. Zhang, C. Li, K. Wang, X. Sun, Y. Ma, High-efficiency sacrificial prelithiation of lithium-ion capacitors with superior energy-storage performance. Energy Storage Mater. **24**, 160–166 (2020)
13. Y.B. An, T. Liu, C. Li, X. Zhang, T. Hu, X.Z. Sun, K. Wang, C. Wang, Y.W. Ma, A general route for the mass production of graphene-enhanced carbon composites toward practical pouch lithium-ion capacitors. J. Mater. Chem. A **9**, 15654 (2021)
14. H. Cheng, C. Ma, W. Li, Facile synthesis of porous $LiMn_2O_4$ nano-cubes for ultra-stable lithium-ion battery cathodes. New. J. Chem. **47**, 5244–5248 (2023)

15. S. Vijayan, B. Kirubasankar, P. Pazhamalai, A.K. Solarajan, S. Angaiah, Electrospun Nd^{3+}-Doped $LiMn_2O_4$ Nanofibers as High-Performance Cathode Material for Li-Ion Capacitors. ChemElectroChem 4, 2059–2067 (2017)
16. L. Liu, X. Diao, Z. He, Y. Yi, T. Wang, M. Wang, J. Huang, X. He, X. Zhong, K. Du, High-performance all-inorganic portable electrochromic Li-ion hybrid supercapacitors toward safe and smart energy storage. Energy Storage Mater. **33**, 258–267 (2020)
17. P. Hou, J. Feng, Y. Wang, L. Wang, S. Li, L. Yang, S.H. Luo, Study on the properties of Li_2MnSiO_4 as cathode material for lithium-ion batteries by sol-gel method. Ionics. **26**, 1611–1616 (2020)
18. Y. Lian, Z. Xu, D. Wang, Y. Bai, C. Ban, J. Zhao, H. Zhang, Nb_2O_5 quantum dots coated with biomass carbon for ultra-stable-lithium-ion supercapacitors. J. Alloy Compd. **850**, 156808 (2021)
19. H. Wang, C. Guan, X. Wang, H.J. Fan, Energy and Power Li-Ion Capacitor based on a TiO_2 nanobelt array anode and a Graphene Hydrogel Cathode. Small. **11**, 1470–1477 (2015)
20. M. Arnaiz, C. Botas, D. Carriazo, R. Mysyk, F. Mijangos, T. Rojo, J. Ajuria, E. Goikolea, Reduced graphene oxide decorated with SnO_2 nanoparticles as negative electrode for lithium ion capacitors. Electrochim. Acta. **284**, 542–550 (2018)
21. S. Sahoo, K. Krishnamoorthy, P. Pazhamalai, V.K. Mariappan, S.J. Kim, Copper molybdenum sulfide nanoparticles embedded on graphene sheets as advanced electrodes for wide temperature-tolerant supercapacitors. Inorg. Chem. Front. **6**, 1775–1784 (2019)
22. P.A. Shinde, N.R. Chodankar, H.J. Kim, M.A. Abdellkareem, A.A. Ghaferi, Y.K. Han, A.G. Olabi, K. Ariga, Ultrastable 1T-2H WS_2 heterostructures by Nanoarchitectonics of Phosphorus-Triggered Phase Transition for Hybrid Supercapacitors. ACS Energy Lett. **8**, 4474–4487 (2018)
23. P.A. Shinde, Q. Abbas, N.R. Chodankar, K. Ariga, M.A. Abdelkareem, A.G. Olabi, Strengths, weaknesses, opportunities, and threats (SWOT) analysis of supercapacitors: a review. J. Energy Chem. **79**, 611–638 (2023)
24. P.A. Shinde, K. Ariga, Two-Dimensional Nanoarchitectonics for two-dimensional materials: Interfacial Engineering of Transition-Metal Dichalcogenides. Langmuir. **39**, 18175–18186 (2023)
25. P.A. Shinde, N.R. Chodankar, M.A. Abdelkareem, S.J. Patil, Y.K. Han, K. Elsaid, Olabi, all Transition Metal Selenide Composed High-Energy Solid-State Hybrid Supercapacitor. Small. **18**, 2200248 (2022)
26. X. Chen, W. Tang, L. Cai, Y. Zhu, S. Peng, X. Li, X. Hu, L. Qiao, S. Liu, Superdispersed $NiCo_2S_4$ nanoparticles anchored on reduced graphene oxide for efficient hydrogen evolution reaction in acidic and alkaline media. J. Alloy Compound. **918**, 165757 (2022)
27. M. Wang, W. Tang, S. Liu, X. Liu, X. Chen, X. Hu, L. Qiao, Y. Sui, Design of earth-abundant ternary $Fe_{1-x}Co_xS_2$ on RGO as efficient electrocatalysts for hydrogen evolution reaction. J. Alloy Compound. **862**, 158610 (2021)
28. J. Zhang, H. Zhang, Y. Zhang, J. Zhang, H. He, X. Zhang, J.J. Shim, S. Zhang, Unveiling of the energy storage mechanisms of multi -modified (Nb_2O_5@C)/rGO nanoarrays as anode for high voltage supercapacitors with formulated ionic liquid electrolytes. Electrochim. Acta. **313**, 532–543 (2019)
29. Q. Deng, Y. Fu, C. Zhu, Y. Yu, Niobium-based oxides toward advanced electrochemical energy storage: recent advances and challenges. Small. **15**, 1804884 (2019)
30. S.P. Varghese, B. Babu, R. Prasannachandran, R. Antony, M.M. Shaijumon, Enhanced electrochemical properties of Mn_3O_4/graphene nanocomposite as efficient anode material for lithium ion batteries **780**, 588–596 (2019)
31. D.P. Dubal, D.S. Dhawale, R.R. Salunkhe, S.M. Pawar, C.D. Lokhande, A novel chemical synthesis and characterization of Mn_3O_4 thin films for supercapacitor application. Appl. Surf. Sci. **256**(14), 4411–4416 (2010)
32. L. Li, Z.A. Hu, N. An, Y.Y. Yang, Z.M. Li, H.Y. Wu, Facile synthesis of MnO_2/CNTs composite for Supercapacitor electrodes with Long Cycle Stability. J. Phys. Che C **118**, 22865–22872 (2014)
33. Y. Zhu, D. Wang, X. Yan, Y. Li, W. Zhou, X. Cheng, B. Geng, Rational design for Mn_3O_4@carbon foam nanocomposite with 0D@3D structure for boosting Electrochemical Performance. Energy Fuels. **34**(11), 14924–14933 (2020)
34. Y. Qin, B. Wang, S. Jiang, Q. Jiang, C. Huang, H.C. Chen, Strongly anchored MnO nanoparticles on graphene as high-performance anode materials for lithium-ion batteries. Ionics. **26**(7), 3315–3323 (2020)
35. C. Liu, Y. Chen, W. Huang, Y. Situ, H. Huang, Birnessite manganese oxide nanosheets assembled on ni foam as high-performance pseudocapacitor electrodes: Electrochemical oxidation driven porous honeycomb architecture formation. Appl. Surf. Sci. **458**, 10–17 (2018)
36. C. Liu, Y. Chen, X. Sun, B. Chen, Y. Situ, H. Huang, The effect of electrolyte cation on electrochemically induced activation and capacitive performance of Mn_3O_4 electrodes. Electrochim. Acta. **324**, 134894 (2019)
37. T.A. Babkova, H. Fei, N.E. Kazantseva, I.Y. Sapirina, P. Saha, Enhancing the supercapacitor performance of flexible MnOxCarbon cloth electrodes by Pd-decoration. Electrochim. Acta. **272**, 1–10 (2018)
38. C. Liu, Q.Q. Ren, S.W. Zhang, B.S. Yin, L.F. Que, L. Zhao, X.L. Sui, F.D. Yu, X. Li, D.M. Gu, Z.B. Wang, High Energy and Power Lithium-Ion Capacitors based on Mn_3O_4/3D-Graphene as Anode and activated polyaniline-derived Carbon Nanorods as Cathode. Chem. Eng. J. **370**, 1485–1492 (2019)
39. F. Gao, J. Qu, Z. Zhao, Q. Zhou, B. Li, J. Qiu, A green strategy for the synthesis of graphene supported Mn_3O_4 nanocomposites from graphitized coal and their supercapacitor application. Carbon. **80**, 640–650 (2014)
40. D. Tie, S. Huang, J. Wang, J. Ma, J. Zhang, Y. Zhao, Hybrid energy storage devices: advanced electrode materials and matching principles. Energy Storage Mater. **21**, 22–40 (2019)
41. H. Liu, X. Liu, S. Wang, H.K. Liu, L. Li, Transition metal based battery-type electrodes in hybrid supercapacitors: a review. Energy Storage Mater. **28**, 122–145 (2020)
42. Z. Li, Z.H. He, J.F. Hou, J.F. Gao, L.B. Kong, Coprecipitation Prepared High-Performance Anode Material $KMnF_3$ for Lithium-Ion Capacitors. Energy Technol. **11**(11), 2300585 (2023)
43. D. Sui, M. Wu, Y. Liu, Y. Yang, H. Zhang, Y. Ma, L. Zhang, Y. Chen, High performance Li-ion capacitor fabricated with dual graphene-based materials. Nanotechnology. **32**, 015403 (2020)
44. H. Wang, L.F. Cui, Y. Yang, H.S. Casalongue, J.T. Robinson, Y. Liang, Y. Cui, H. Dai, ChemInform Abstract: Mn_3O_4-Graphene hybrid as a high-capacity Anode Material for Lithium Ion batteries. Cheminform. **132**, 13978–13980 (2010)
45. L. Chen, W. Zhai, L. Chen, D. Li, X. Ma, Q. Ai, X. Xu, G. Hou, L. Zhang, Nanostructured $LiMn_2O_4$ composite as high-rate cathode for high performance aqueous Li-ion hybrid supercapacitors. J. Power Sources. **392**, 116–122 (2018)
46. L. Chen, L. Chen, W. Zhai, D.Y. Li, S. Lin, J. Guo, L. Feng, P. Zhang, L. Si, L. Song, J. Ci, Tunable synthesis of $LixMnO_2$ nanowires for aqueous Li-ion hybrid supercapacitor with high rate capability and ultra-long cycle life. J. Power Sources. **413**, 302–309 (2019)
47. Z. Chen, V. Augustyn, J. Wen, Y. Zhang, M. Shen, B. Dunn, Y. Lu, High-performance supercapacitors based on intertwined CNT/V_2O_5 Nanowire nanocomposites. Adv. Mater. **23**(6), 791–795 (2011)

48. Y. Ren, J. Li, J. Guo, Perforated active Carbon and Pre-lithiated Graphite electrodes for high performance hybrid Lithium-ion Capacitors. Int. J. Electrochem. Sci. **15**, 2659–2666 (2020)
49. C. Sun, X. Zhang, C. Li, K. Wang, X. Sun, Y. Ma, High-efficiency sacrificial prelithiation of lithium-ion capacitors with superior energy-storage performance. Energy Storage Mater. **24**, 160–166 (2019)
50. Q. Qin, L. Chen, T. Wei, X. Liu, MoS_2/NiS yolk–Shell Microsphere-based electrodes for overall water splitting and asymmetric supercapacitor. Small. **15**(29), 1803639 (2019)